ENGINEERING

Battery-free, fully implantable optofluidic cuff system for wireless optogenetic and pharmacological neuromodulation of peripheral nerves

Yi Zhang[1,2]*, Aaron D. Mickle[3,4]*, Philipp Gutruf[5,2]*, Lisa A. McIlvried[3,4]*, Hexia Guo[2], Yixin Wu[2], Judith P. Golden[3,4], Yeguang Xue[6,7], Jose G. Grajales-Reyes[3,4], Xueju Wang[8], Siddharth Krishnan[2], Yiwen Xie[2], Dongsheng Peng[2,9], Chun-Ju Su[2], Fengyi Zhang[10], Jonathan T. Reeder[2], Sherri K. Vogt[3,4], Yonggang Huang[2,6,7], John A. Rogers[2,11,12,13,14,15]†, Robert W. Gereau IV[3,4,16]†

Studies of the peripheral nervous system rely on controlled manipulation of neuronal function with pharmacologic and/or optogenetic techniques. Traditional hardware for these purposes can cause notable damage to fragile nerve tissues, create irritation at the biotic/abiotic interface, and alter the natural behaviors of animals. Here, we present a wireless, battery-free device that integrates a microscale inorganic light-emitting diode and an ultralow-power microfluidic system with an electrochemical pumping mechanism in a soft platform that can be mounted onto target peripheral nerves for programmed delivery of light and/or pharmacological agents in freely moving animals. Biocompliant designs lead to minimal effects on overall nerve health and function, even with chronic use in vivo. The small size and light weight construction allow for deployment as fully implantable devices in mice. These features create opportunities for studies of the peripheral nervous system outside of the scope of those possible with existing technologies.

INTRODUCTION

Pharmacology and optogenetics represent two distinct, and often complementary, approaches that are widely used in neuroscience research (*1*–*10*). Optogenetics allows for light-dependent activation or inhibition of function in genetically defined neuronal populations, with the ability to manipulate and study discrete neuronal circuits (*1*, *8*, *11*). Pharmacology can target specific cellular process, from cell surface receptor or ion channel function to intracellular signaling, without the need for genetic modifications. Protocols for interrogating neural circuits while measuring subtle animal behaviors with either of these methods are, however, often restricted by limitations of the supporting hardware technologies, especially for studies of freely moving small animals. For example, traditional optogenetic assays rely on fiber-optic cables coupled to external light sources (*12*). In vivo pharmacological studies require tubing that connects to separate reservoirs and micropumps, or they require syringe injections while the animals are physically restrained and/or anesthetized. These approaches can (i) damage sensitive tissues during injection or implantation, (ii) cause persistent irritation at the biotic/abiotic interface due to mechanical interaction between the delivery hardware and the surrounding soft, moving tissues, and (iii) introduce physical constraints on the natural movements of the animals, thereby affecting or preventing free motions and increasing stress and anxiety (*13*–*16*). These technical shortcomings limit options in experimental design and can confound the interpretation of experimental results.

Efforts to address these limitations have advanced in optogenetics, where a variety of systems based on microscale light-emitting diodes and wireless powering strategies are now available (*17*–*20*). Devices for the peripheral nervous system (PNS) can broadly illuminate sensory neuron peripheral terminals in large structures (*17*, *18*, *21*) or the central terminals projecting into the spinal cord (*17*, *18*, *20*). Challenges persist, however, in noninvasive methods for (i) securing the devices to the PNS or adjacent anatomical structures and (ii) enabling sufficient mechanical compliance to accommodate the movements that occur in awake behaving animals. Difficulties in establishing pharmacological interfaces with peripheral nerves are even more pronounced, particularly in small animals. Currently available methods for drug delivery via catheters or syringes do not address these confounds. Recently reported battery-powered, wireless, head-mounted optofluidic platforms anchor to rigid parts of the anatomy such as the skull for studies of the brain (*10*). Certain features, however, prevent their use for interfacing with the PNS: (i) Thermal-mechanical actuation of the microfluidic pumps demands substantial power, thereby requiring batteries with sizes and weights (0.66 g) that are nonideal for the full implantation in mice; (ii) the heat generated during the operation of these micropumps could degrade temperature-sensitive pharmacological agents, thereby restricting the range of uses; (iii) functional lifetime depends on the

[1]Department of Biomedical, Biological, and Chemical Engineering, University of Missouri, Columbia, MO 65211, USA. [2]Department of Materials Science and Engineering, Northwestern University, Evanston, IL 60208, USA. [3]Washington University Pain Center and Department of Anesthesiology, Washington University, St. Louis, MO 63110, USA. [4]Washington University School of Medicine, 660 S. Euclid Ave., Box 8054, St. Louis, MO 63110, USA. [5]Biomedical Engineering, College of Engineering, The University of Arizona, Bioscience Research Laboratories, 1230 N. Cherry Ave., Tucson, AZ 85721, USA. [6]Department of Civil and Environmental Engineering, Northwestern University, Evanston, IL 60208, USA. [7]Department of Mechanical Engineering, Northwestern University, Evanston, IL 60208, USA. [8]Department of Mechanical and Aerospace Engineering, University of Missouri, Columbia, MO 65211, USA. [9]College of Optoelectronic Engineering, Shenzhen University, Shenzhen 518060, China. [10]School of Chemical and Biomolecular Engineering, Georgia Institute of Technology, Atlanta, GA 30318, USA. [11]Simpson Querrey Institute, Northwestern University, Chicago, IL 60611, USA. [12]Center for Bio-Integrated Electronics, Northwestern University, Evanston, IL 60208, USA. [13]Department of Biomedical Engineering, Northwestern University, Evanston, IL 60208, USA. [14]Department of Chemistry, Northwestern University, Evanston, IL 60208, USA. [15]Department of Neurological Surgery, Feinberg School of Medicine, Northwestern University, Chicago, IL 60611, USA. [16]Departments of Neuroscience and Biomedical Engineering, Washington University, St. Louis, MO 63110, USA.
*These authors contributed equally to this work.
†Corresponding author. Email: jrogers@northwestern.edu (J.A.R.); gereaur@wustl.edu (R.W.G.)

battery capacity, thereby preventing chronic, longitudinal studies; and (iv) the absence of a means to refill the microfluidic chambers prevents the reuse of the systems. These shortcomings motivate the design of a new microfluidic fluid delivery system for use in chronic in vivo studies of the PNS.

Here, we present a wireless, battery-free, fully implantable device with the capability for programmed delivery of localized optical and/or pharmacological stimuli, designed to eliminate key disadvantages of previously reported approaches. The device includes an ultralow-power, miniaturized electrochemical micropump system to drive fluid delivery via microfluidic channels incorporated in a soft optofluidic cuff that surrounds a targeted nerve. Operation of these devices occurs in freely moving animals, without the need for handling or physical manipulation. We show that these devices remain in position without signs of damage to the nerves 10 weeks after implantation. In vivo studies demonstrate the capabilities to positively (optogenetic stimulation) and negatively (bupivacaine delivery) modulate nociception in freely behaving mice. The ability to target specific peripheral neuron populations in awake behaving animals, over extended periods of time, is of broad potential interest to the neuroscience community.

RESULTS

Design of the wireless, battery-free optofluidic cuff system

The device consists of six subsystems: (i) a low-modulus (~3 MPa), elastomeric cuff that supports chronic interfacing with peripheral nerves; (ii) a thin microfluidic channel structure (four channels each with cross-sectional areas of 60 μm by 60 μm; total thickness, ~200 μm) that terminates at the cuff for targeted delivery of pharmacological agents (i.e., drugs) at the cuff-nerve interface; (iii) a high-efficiency, microscale inorganic light-emitting diode (μ-ILED; 270 μm by 220 μm by 50 μm) that also resides in the cuff for delivering light at the target location; (iv) a base station (radius, 5 mm; thickness, ~4 mm) that contains fluid reservoirs, programmable pumping microsystems, and hardware for wireless power harvesting, control, and management; (v) a mechanically compliant, serpentine electronic interconnect joining the μ-ILED to the base station (Fig. 1, A to E); and (vi) a collection of external hardware and software systems for independent, wireless control over the μ-ILED and microfluidics (fig. S1). In the device described here, four miniaturized electrochemical micropumps, selected because of their low power consumption and negligible heat generation, couple to a corresponding set of reservoirs to initiate the flow of drugs at user-selected times (Fig. 1E). The small size and light weight (~0.3 g) of this integrated system allow for complete implantation, even into small animals such as mice. Fully wireless operation eliminates the need to directly handle, anesthetize, or inject the animals after the initial implantation, thereby avoiding stress and/or pain that could otherwise lead to experimental artifacts in behavioral testing.

Wireless energy harvesting and power management occur through an electronics module that uses resonant near-field coupling and custom control software (*22*). Here, power transfer follows from magnetic inductive coupling at a frequency of 13.56 MHz, matched to near-field communication (NFC) interfaces found in consumer electronics and also in recently reported devices for optogenetics (*19*–*21*). Operation is compatible with many environments, including cages with metal plates or meshes and arenas with water pools or mazes. Further, the system can operate over large areas (thousands of square centimeters) (*19*). A thin, flexible printed circuit board serves as a substrate for a radio frequency (RF) coil antenna, a set of capacitors, a rectifier, and a microcontroller (Fig. 1, E and F, and fig. S1, A and B). The rectifier includes a matching capacitor (82 pF) to support resonant operation at 13.56 MHz and two Schottky diodes to rectify the received RF signals. Programmable control over a separate micropump for each reservoir occurs through a microcontroller that activates by amplitude shift keying, in a manner compatible with the control hardware (Fig. 1F) (*23*). The complete system includes a software interface, a multicomponent power distribution control box, an antenna tuner, and a customizable antenna (fig. S1C).

Ultralow-power, miniaturized electrochemical micropumps

The ultralow-power, miniaturized electrochemical micropumps represent key components of the system. In general, micropump actuation can be achieved with osmotic pressure, fluorocarbon propellants, electromagnetic forces, piezoelectric transducers, electrostatic impellers, thermopneumatic effects, and electrochemical methods (*24*–*27*). The electrochemical method, as implemented in the form of water electrolysis, is used because of its low power consumption, small physical size, minimal heat generation, simple construction, and large driving force (*24*–*27*). These features represent important advantages over battery-powered thermomechanical micropumps reported in optofluidic devices designed for use in the brain (*10*). The specific layout includes a pumping chamber (radius, 1.2 mm; height, 1 mm) filled with an aqueous solution of potassium hydroxide (KOH; 50 mM) with an interdigitated electrode (Au/Cu: thickness, 200 nm/18 μm; width, ~50 μm; space, ~50 μm) at its base (fig. S2) and an overlying reservoir filled with a drug, where a flexible membrane separates the chamber from the reservoir (Fig. 2, A and B). The gold coating prevents corrosion of the copper electrodes. The flexible membrane consists of a thin film of polystyrene-block-polybutadiene-block-polystyrene (SBS; ~150 μm), chosen because of its favorable mechanical properties and effective barrier characteristics (fig. S3 and table S1). Thin membranes of metal/Al_2O_3 (thickness, ~425 nm) seal the outlet ports of the reservoirs to prevent leakage or evaporation of drugs before infusion (Fig. 1E). An opening on the sidewall of each reservoir allows for replenishment of drugs, thereby enabling multiple cycles of use (Fig. 1E). Removable layers of silicone elastomer (Kwik-Sil) seal the ports after filling.

Each reservoir connects to a microfluidic channel that terminates at an outlet integrated into the cuff (Fig. 1, D and E). The micropump chamber and reservoir are both milled from a block of cyclic olefin polymer (COP; thickness, 1 mm), selected for its low water absorption (<0.01%); resistance to hydrolysis, acids, alkalis, and polar solvents; and efficiency as a moisture barrier (water vapor permeability, 0.023 g·mm/m^2·day) (*10*, *28*). At 37°C, the rates of fluid loss due to diffusion into the COP are minimal, which is critical for chronic, long-term studies (Fig. 2C). Voltage applied to the interdigitated electrodes in the pumping chamber initiates electrolysis via the reaction $2H_2O$ (liquid) → O_2 (gas) + $2H_2$ (g) (*24*, *26*). An electrolyte solution of 50 mM KOH provides sufficient conductivity. The volume expansion associated with the production of hydrogen and oxygen mechanically deforms the flexible membrane (Fig. 2, A, B, and D, and movie S1). This deformation drives the flow of drug from the reservoir, through the microfluidic channel, and out of the corresponding outlet at the cuff (Fig. 2B and movie S2).

The pressure increases with time after activation of the micropump, as the generated gases accumulate in the sealed micropump chamber.

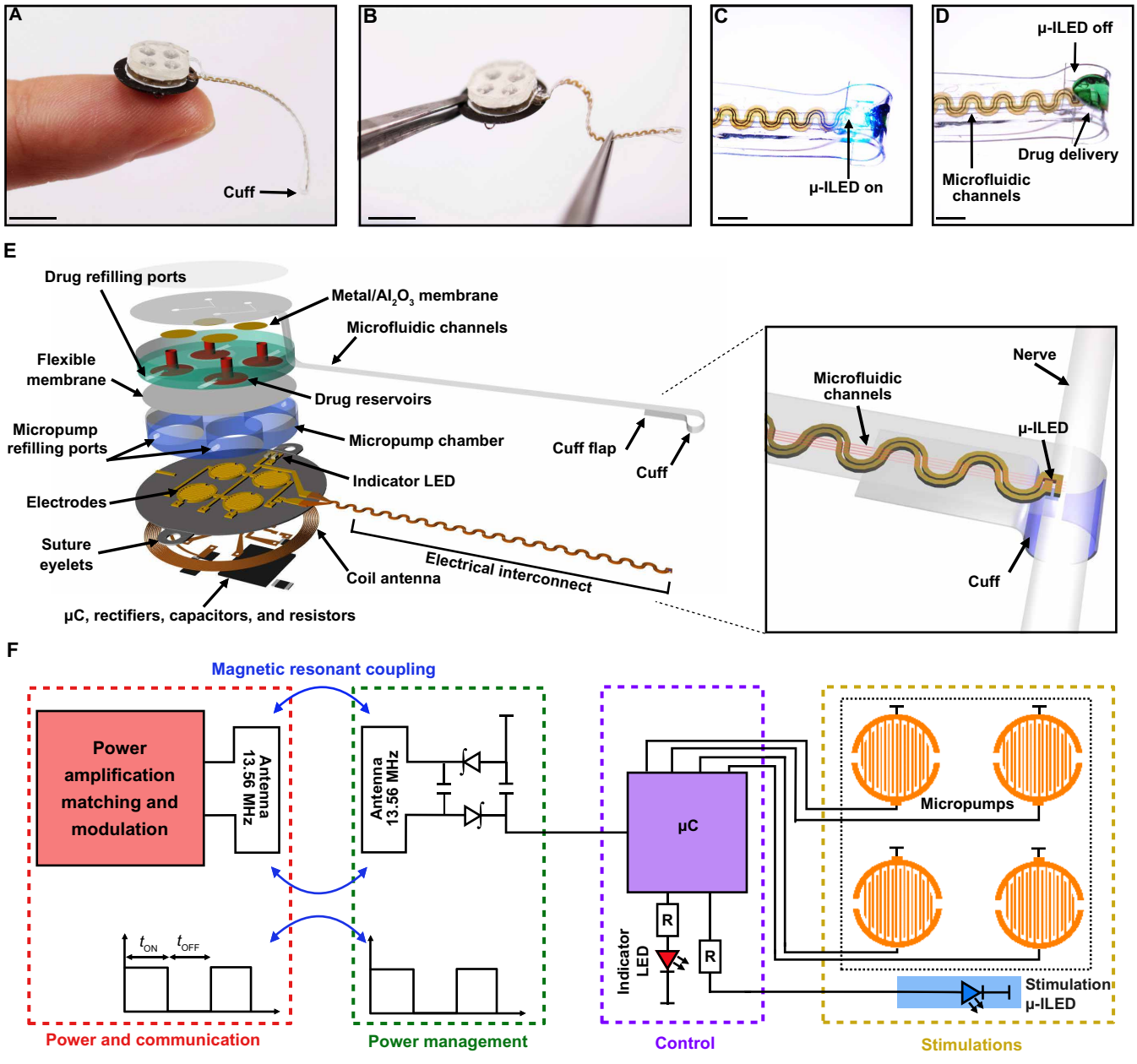

Fig. 1. Wireless, battery-free neural cuff for programmable pharmacology and optogenetics. (**A** and **B**) Demonstrations of the overall size of the system. Scale bars, 5 mm. (**C** and **D**) Magnified views of the neural cuff interface with optical μ-ILED activation and fluid delivery. Scale bars, 1 mm. Exploded view (**E**) and electrical schematic diagram (**F**) of the wireless optofluidic system for programmable pharmacology and optogenetics. μC, microcontroller.

Under typical operating conditions (applied current, 0.3 mA), the pressure reaches ~108 kPa at the state of maximum deformation of the membrane, as the drug is completely expelled from the reservoir (1.5 μl; fig. S4). The pressure inside the micropump chamber is mostly cancelled by deformation of the membrane, resulting in a much lower pressure (~7 kPa) in the drug reservoir (fig. S4). The bottom polyimide (PI) substrate barely deforms during this process as it is much stiffer (2.5 GPa) than the soft membrane (~13 MPa). Some of the pressure is released by transport of gases, primarily hydrogen, through the membrane. The remaining pressure remains in the micropump chamber until refilling. This pressure can be released by peeling off the removable layers of silicone elastomer (Kwik-Sil). Although a small amount of oxygen or hydrogen may pass through the SBS flexible membrane, their influence on the drugs is minimal (*29*).

The wireless powering system generates ~15 mW from a ~1-cm-diameter receiver coil (*19*), which is more than sufficient for full fluid delivery and μ-ILED illumination (Fig. 2E). The ultralow power consumption of electrochemical micropumps (Fig. 2E), compared with the battery-powered thermomechanical micropumps (*10*), enables wireless, battery-free operation, allowing the platform to operate with a much smaller size and weight than available alternatives. The removal of a battery component decreases overall device size, permitting full implantation under the skin. The wireless powering system eliminates any concern about operational longevity. While batteries

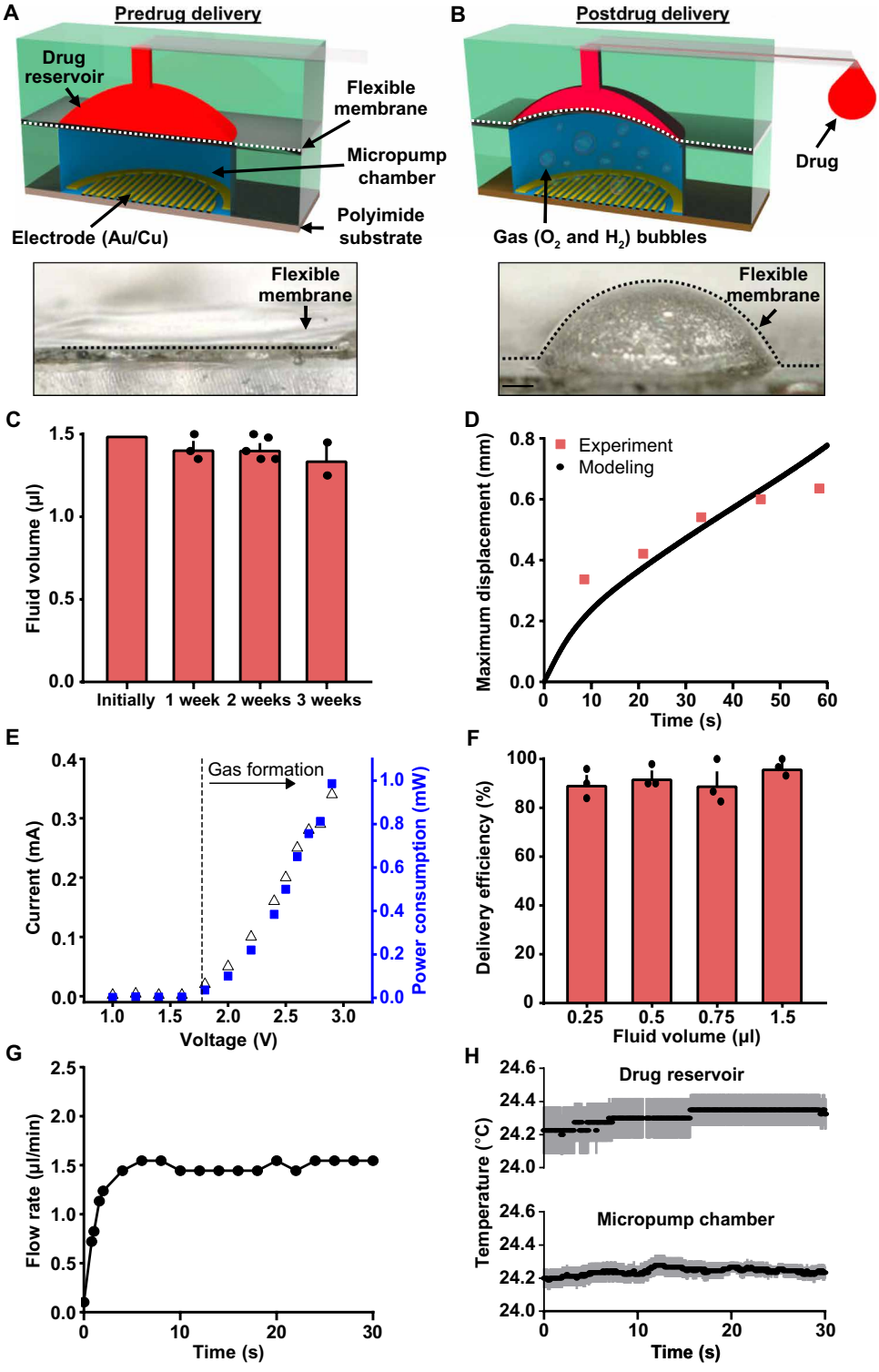

Fig. 2. Fluidic and electrical characteristics of the wireless optofluidic system. (**A** and **B**) Top: Schematic diagram of the electrochemical micropump. Applying current to a pair of electrodes initiates pumping through expansion induced by electrochemical phase change of liquid water into hydrogen and oxygen gases. The resulting pressure in the micropump chamber deforms the flexible membrane and delivers the drug. Bottom: Images of mechanical deformation of the flexible membrane induced by water electrolysis. Scale bar, 0.3 mm. (**C**) Fluid volume in the drug reservoir as a function of time. (**D**) Comparison between experiment and modeling of maximum displacement of flexible membrane induced by water electrolysis. (**E**) Current-voltage-power characteristics of the electrochemical micropump. (**F**) Total infusion efficiency from various loaded volumes in representative devices ($n = 3$ devices). (**G**) Flow rate in a microfluidic channel as a function of time. (**H**) Temperature of the drug chamber (top) and micropump chamber (bottom) during the electrochemical pumping process (3 V). All data are represented as means ± SEM.

can provide robust power supplies, the constraints imposed to keep them small result in short life spans, making them difficult to use for extended behavioral experiments.

Experimental evidence indicates that ~90% of the reservoir volume is delivered through the outlet at the cuff (Fig. 2F). At a voltage of ~3 V, a device with channel cross-sectional dimensions of 60 μm by 60 μm has a flow rate of ~1.5 μl/min (Fig. 2G), without any measurable heating (Fig. 2H), which is an substantial advantage over previous technology, as heating can be detrimental to drug stability and efficacy (*10*). The flow rate is tuned by the applied voltage and by engineering the geometries of the reservoirs and channels. The pumping mechanisms, electrode designs, and refilling ports allow for reuse of the microfluidic system (fig. S5). In this process, the electrolyte solution (50 mM KOH in water) and drugs can be loaded with syringes into the micropump chamber and drug reservoir, respectively, through the filling ports (fig. S5A) that are subsequently sealed. Figure S5B shows a system loaded before implantation and extracted after drug delivery in vivo.

Design and material properties of the soft neural cuff

The cuff interface consists of an elastomeric polymer [poly(dimethylsiloxane), PDMS] that is thin (~200 μm), mechanically soft, and flexible (modulus, ~3 MPa). The cuff is designed to minimize its effects on overall nerve health by using comparable mechanical properties with peripheral nerve tissue (mouse sciatic nerve modulus, ~7 MPa) (*30*). Microfluidic channels and a μ-ILED (on a narrow, thin strip of PI with copper interconnect traces) embedded in the PDMS support the pharmacologic and optogenetic functionality of the system (Fig. 1, C to E). The serpentine shape of the PI filament that connects the cuff to the base station ("electrical interconnect") provides mechanical stretch (~15 to 20%) to accommodate natural body movements (fig. S6, A and B). The stress-strain response of the optofluidic probe (integrated electrical interconnect, microfluidic channels, and cuff), evaluated by dynamic mechanical analysis, indicates an effective modulus of ~25 MPa (fig. S6C), higher than that of the cuff itself. Operation of the μ-ILEDs elevates the temperature of the nerve only slightly (maximum increase of 0.85°C with constant illumination over 5 min), below thresholds for damage (fig. S7) (*31*).

The cuff is designed to form a cylindrical shape that wraps around the nerve (Fig. 1E). This geometry results from bonding two flat, thin strips of PDMS by corona treatment, one of which is in a state of prestrain (fig. S8, A to D). Releasing this prestrain yields a cylindrical shape with a radius that decreases with increasing prestrain, χ. The critical value χ_{cr} required to form a cuff with inner radius R_{nerve} is shown in fig. S9A. In practice, the value of χ is typically larger than χ_{cr} such that the cuff has a radius somewhat smaller than R_{nerve}, leading to a modest contact pressure with the nerve to hold the cuff in place (fig. S9B). Results of analytical modeling indicate that the average contact pressure can be controlled to values below 7 kPa, a threshold for damage to the sciatic nerve in mice (*30*), by use of a prestrain less than 38%. Experiments reported here involve prestrains of 30% (fig. S9C).

Effects of the optofluidic system on nerve health and function

The full optofluidic system was chronically implanted in mice to determine its effects on nerve health and function. In a single surgical procedure, the base station was secured over the thoracic curve of the vertebral column using two sutures through integrated eyelets to the underlying muscle. The cuff was then wrapped around the sciatic nerve, and the flap was fastened to the cuff lead (Fig. 3, A to C). One week after implantation, mice with the implant do not exhibit any behavioral indications of nerve damage compared to animals with a sham surgery, as measured through analysis of gait properties and locomotor coordination (Fig. 3, D to G; $n = 9$ sham; $n = 10$ device implantation). Two weeks after implantation, the cuff remains in its original position, with no signs of degradation in functionality (Fig. 3C and fig. S10, A and B; $n = 10$ device implantation). By comparison, a polyethylene (PE) tubing cuff results in clear deficits in coordination and changes gait parameters of the ipsilateral limb (Fig. 3, D to G; $n = 8$ to 10 PE cuffs). Compared to the optofluidic cuff system, the PE cuff has a relatively high modulus (~0.25 GPa) (*32*–*34*), and the inability of the PE cuff to conform to the curvature and motions of the soft tissues results in injury to the nerve (*35*). Mice with an implanted PE cuff (fig. S10C) also show a significant increase in immune cell infiltration in the sciatic nerve compared to either the optofluidic cuff system or sham animals (Fig. 3, H and I; $n = 3$ in each group).

In vivo demonstration of the optogenetic and microfluidic capabilities of the optofluidic system

Two different animal experiments illustrate the capabilities of this system. The first demonstrates the μ-ILED functionality in vivo and its ability to activate within a specific region of the experimental arena. Here, we used mice that express channelrhodopsin2 (ChR2), an excitatory opsin activated by blue light, in nociceptors (TRPV1-ChR2 mice; see Materials and Methods). Optical stimulation (470 nm; blue light) of these neurons results in aversive behavior (*18*). One week after implantation, unilateral sciatic nerve stimulation with blue light at 1 Hz (pulse width, 10 ms), but not at 10 Hz, induces significant aversion to the stimulation chamber in TRPV1-ChR2 mice compared to wild-type mice (Fig. 4, A to C; $n = 10$ wild type; $n = 9$ TRPV1-ChR2).

The second set of experiments demonstrates both temporally defined fluid delivery to the sciatic nerve in vivo and the ability to deliver multiple drugs to the same animal without handling the animal between treatments. Here, two reservoirs (each with volumes of 1.5 μl) of the system contain saline and the other two contain bupivacaine (40 mg/ml), a nonspecific voltage-gated sodium channel blocker and local anesthetic. Five days after implantation, we assessed thermal paw withdrawal thresholds at baseline, after saline, and after bupivacaine delivery (Fig. 4D). Delivery of bupivacaine significantly increases withdrawal latency compared to both baseline and saline, indicating a decreased thermal sensitivity and induction of a sciatic nerve block, with no other indications of systemic effects (Fig. 4E; $n = 6$ in baseline and saline; $n = 5$ in bupivacaine).

DISCUSSION

The wireless, battery-free, soft, fully implantable optofluidic cuff system reported here allows for long-term modulation of peripheral nerve activity via operation of a microfluidic system for localized drug delivery and a cointegrated μ-ILED for optogenetic stimulation. Critically, the system's soft cuff interface does not damage the associated peripheral nerve and permits targeted delivery of light, as opposed to broad illumination (*20*, *21*), in a manner that restricts activation

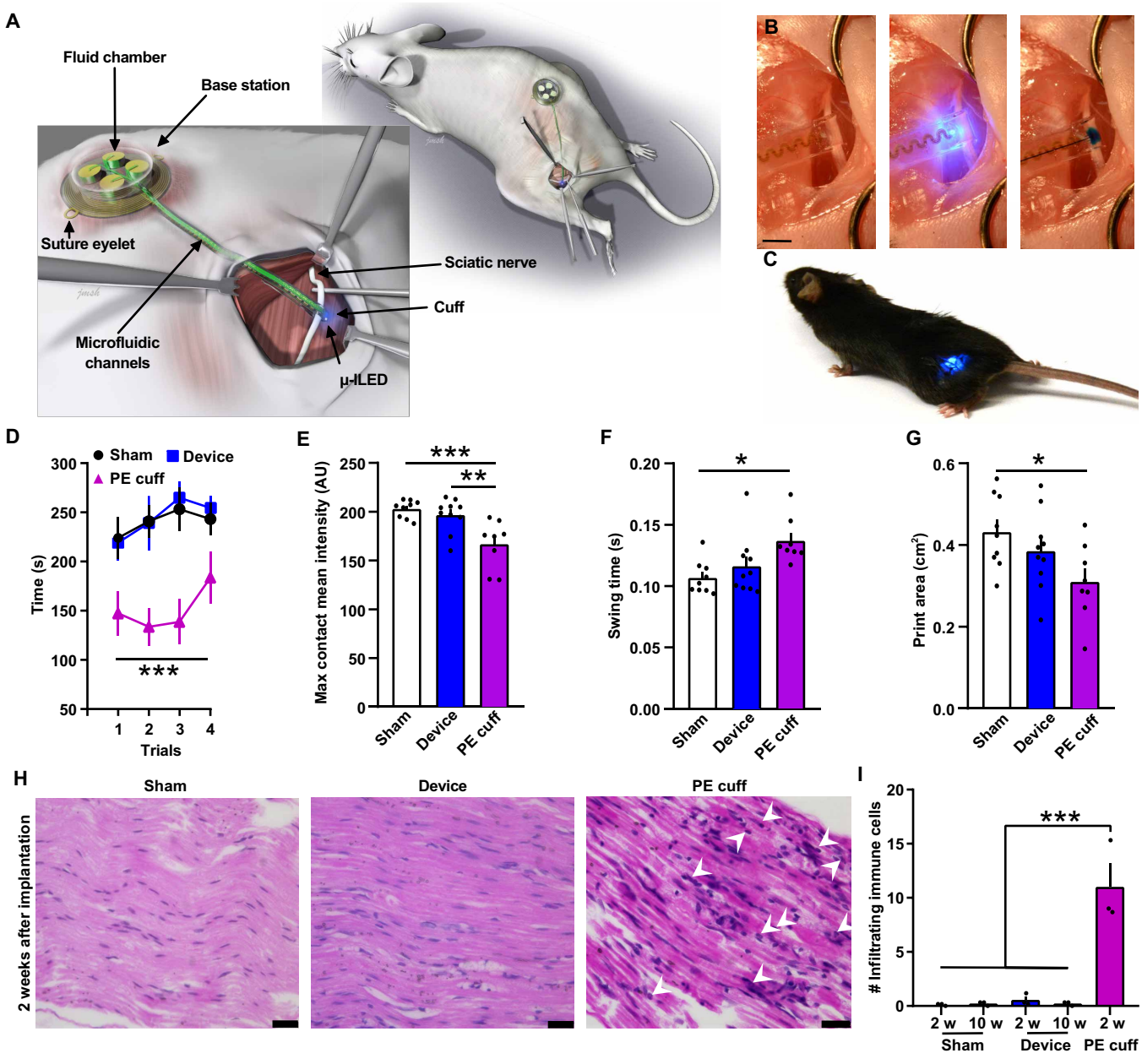

Fig. 3. Implantation of the battery-free optofluidic nerve cuff system and its impact on animal behavior and nerve health. (**A**) Detailed illustration of the optofluidic nerve cuff system and cuff interface with the mouse sciatic nerve. (**B**) Demonstration of both optical stimulation and fluid delivery to the sciatic nerve. Scale bar, 2 mm. (**C**) Mouse chronically implanted with the wirelessly powered optofluidic nerve cuff system. (**D**) Characterization of effects of device implantation on rotarod performance compared to PE cuff and sham surgery [$n = 9$ to 10; $^{***}P < 0.001$ PE cuff versus sham and device, two-way analysis of variance (ANOVA)]. Mouse gait parameters including maximum contact mean intensity (**E**), swing time (**F**), and print area (**G**) are significantly impaired after PE cuff implantation but not after optofluidic cuff implantation compared to sham surgery ($n = 8$ to 10; $^{***}P < 0.001$, $^{**}P < 0.01$, and $^{*}P < 0.05$, one-way ANOVA with Tukey's multiple comparison). Representative hematoxylin and eosin images (**H**) and quantification of infiltrating immune cells (**I**) from the sciatic nerve comparing sham, device, and PE cuff after 2 weeks (w) of implantation demonstrating an absence of infiltrating immune cells in sciatic nerves of mice implanted with the device compared to PE cuff implantation. Scale bars, 25 μm. $n = 3$; $^{***}P < 0.001$, one-way ANOVA with Tukey's multiple comparison. AU, arbitrary units.

of optogenetic channels to a specific nerve. The ultralow-power, miniaturized electrochemical micropump system–driven microfluidic functionality bypasses limitations with traditional fluid delivery technologies by delivering time-locked pharmacological agents to specific nerves without the need to handle, inject, tether, restrain, or anesthetize the animals. In addition, because the system does not rely on batteries, it weighs substantially less than alternatives (*10*) and can be used in long-term experiments. Furthermore, by using NFC powering and communication protocols, the set-up costs and required expertise are markedly less than high-frequency alternatives (*18*, *36*), allowing for high-throughput experiments with lower operation costs.

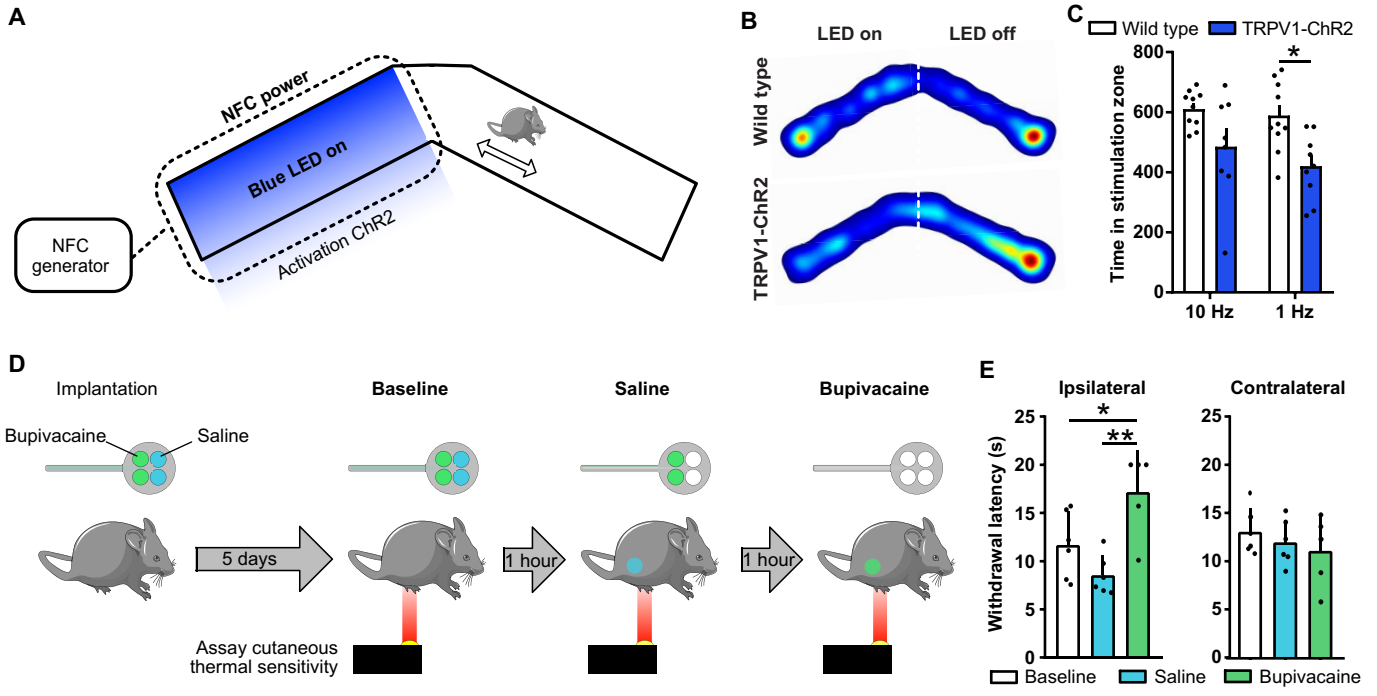

Fig. 4. Demonstration of optogenetic and microfluidic capabilities of the wireless, battery-free optofluidic nerve cuff system. (**A**) Schematic of the real-time place preference assay designed to test the capabilities of nerve cuff optical stimulation. Representative heat maps (**B**) and quantification (**C**) of blue light stimulation of sciatic nerve in wild-type and TRPV1-ChR2 mice. Mice were placed in the chamber for a total of 20 min. TRPV1-ChR2 mice displayed significant aversion to 1-Hz light pulse stimulus compared to wild-type mice ($n = 9$ to 10; $^*P < 0.05$, two-way ANOVA with Sidak's multiple comparisons test). (**D**) Optofluidic cuff devices loaded with bupivacaine and saline were implanted in mice, and thermal sensitivity was assayed before and after saline and again after bupivacaine infusion. (**E**) Quantification of the withdrawal latency to thermal stimulation of the ipsilateral (device side) and contralateral paw at baseline, after saline and after bupivacaine ($n = 5$ to 6; $^*P < 0.05$ and $^{**}P < 0.01$, one-way ANOVA with Sidak's multiple comparisons test).

The capability for independent infusion of multiple drugs allows testing of several drugs in a single animal. For example, vehicle, agonist alone, antagonist alone, and an antagonist and agonist combination can be delivered independently to a single, awake, and behaving animal. In addition, the same drug can be tested before and after an experimental manipulation. This mode of operation not only reduces the number of animals needed for any given experiment but also exploits each animal as its own control, as demonstrated here, to reduce experimental variability.

This same level of independent control over separate reservoirs and micropumps permits drugs to be simultaneously delivered to the nerve surface for time-controlled chemical reactions, of potential interest in combination therapies. In addition, dual optical and pharmacological operation enable studies that use optically activated drugs (*10*, *36*, *37*) and single-step optogenetics (*38*). One limitation of fully implantable drug delivery systems is compound stability at body temperature over extended periods of time. The stability of various compounds can be improved by careful testing of different delivery vehicles and sterilization. Future technology could help improve these conditions by mixing lyophilized compounds on demand or altering the internal temperature of the drug reservoir.

Other systems that provide wireless drug delivery with or without light delivery, such as battery-powered, head-mounted platforms for studies of the brain (*10*), are not easily adaptable for peripheral use. The size and bulk of these platforms prevent them from being fully implanted and are not well suited for interfacing with the PNS. Alternatives include wireless power transfer using RF operation in the UHF (ultrahigh-frequency, 300–3,000 MHz) band (*36*), but this system has disadvantages including tissue absorption, reflections, and sensitivity to orientation and polarization (*39*, *40*). Other platforms use commercially available miniaturized pumps (*3*), battery power, and stainless steel needles, but they cannot be used readily in small animals because of their bulky size.

The system introduced here eliminates many of the substantial disadvantages inherent in previously described technologies. We demonstrate the ability of this platform to positively (optogenetic stimulation) and negatively (bupivacaine delivery) modulate sciatic nerve activity in freely moving animals. In addition, these devices have the potential to target much smaller nerve branches to provide more specific stimulation, such as the pelvic nerve to modulate bladder function (*41*). Furthermore, the core ideas and the supporting technology platforms can be adapted to other non-neuronal or central nervous system structures. For example, the cuff could easily be enlarged to accommodate hollow organs such as the colon, trachea, or esophagus. In addition, more intricate interface architectures could be tailored to target organs such as the heart, liver, or pancreas, each with radically different shapes. This interface could also be adapted into a small flexible probe for placement in the intrathecal space (*18*), to manipulate spinal cord neurons, or designed on a rigid structure for stereotaxic implantation into different brain regions (*10*). Overall, the system introduced here improves the tool set available for advanced manipulation of peripheral nerves in awake, freely moving animals to further characterize and develop functional maps of the PNS.

MATERIALS AND METHODS

Fabrication of the soft nerve cuff

As described in the main text, formation of the cuff relies on effects in controlled mechanical buckling. The fabrication began with spin-coating a precursor to PDMS (10:1 prepolymer/curing agent; 800 rpm for 60 s; Sylgard 184, Dow Corning) on a thin plate (1.5 mm) of polycarbonate (PC) followed by thermal curing. Corona treatment enabled bonding of a strip of PDMS (thickness, 100 μm; width, ~2 mm; length, 1 cm) formed in this way to another piece (thickness, 100 μm; width, ~1.5 mm; length, 3 cm) while under a state of prestrain. Releasing the prestrain led to the formation of a cylindrical shape.

Fabrication of the microfluidic probe

The soft microfluidic probe consists of two layers, a molded microchannel layer and a capping layer, bonded by corona treatment. The fabrication process began with formation of a mold in the geometry of the microfluidic channels by photolithography and deep reactive ion etching (STS Pegasus ICP-DRIE; SPTS Technologies, Newport, UK) on the surface of a silicon wafer. A glass slide (length, 75 mm; width, 50 mm; thickness, 1 mm; Corning Microscope Slides, Corning, NY, USA) treated with a Pt inhibitor, a solution of 5% [3-(2-aminoethylamino) propyl]trimethoxysilane (Sigma-Aldrich, St. Louis, MO, USA), and 95% methanol by weight, facilitated the release of a layer of PDMS (elastomer/curing agent ratio, 10:1; Sylgard 184, Dow Corning) cast between the glass slide and the patterned silicon wafer. A layer of Scotch tape served as a spacer at the boundary of the slide to define the thickness of the PDMS. A thin layer (~60 nm) of polymethyl methacrylate (PMMA A2; MicroChem, MA, USA) spin-cast on the silicon mold served to prevent adhesion between the silicon mold and the PDMS. Curing in an oven at 70°C for 45 min and then carefully releasing the glass slide with the patterned PDMS layer from the silicon mold completed the fabrication of the thin microfluidic channel layer (thickness, ~100 μm). A capping layer of PDMS (thickness, ~100 μm) was prepared by spin-casting (elastomer/curing agent ratio, 10:1; Sylgard 184, Dow Corning) on a PC substrate and baking at 70°C for 45 min. Bonding this cover layer to the microfluidic channel after activating the surfaces with a laboratory corona treater (Electro-Technic Products) yielded a microfluidic probe. The PC sheet was then peeled away, and the probes were released from the glass slide with a razor blade.

Fabrication of the μ-ILED probe

Fabrication began with a clean glass slide (length, 75 mm; width, 50 mm; thickness, 1 mm; Corning Microscope Slides, Corning, NY, USA) coated with PDMS formed by spin-casting at 1000 rpm for 60 s followed by curing at 70°C for 1 hour. A sheet of copper-coated PI (9 μm/12 μm, copper/PI) was then laminated on top. Photolithography (AZ 5214, AZ Electronic Materials) and wet etching defined a pattern of copper traces. A 12-μm-thick layer of PI (PI-2545, HD MicroSystems), formed by spin-casting and curing at 250°C for 2 hours, served as an encapsulation layer and a means to locate the copper near the position of the neutral mechanical plane. Photolithography and reactive ion etching then defined the PI/metal/PI sheet into serpentine-shaped structures. A μ-ILED (TR2227, Cree Inc.) was placed onto the exposed pads with a small amount of solder paste (Indalloy 290, 97.0In/3.0Ag, Indium Corporation). The resulting probe was released from the glass substrate by laser cutting of the patterned PI/metal/PI sheet (ProtoLaser U4, LPKF, Germany).

Finite element analysis of the optofluidic probe

Three-dimensional finite element analysis was performed using commercial software Abaqus to study the deformation and strain in the serpentine wire under stretching. Solid elements (Abaqus element type C3D8R) were used for the 300-μm-thick PDMS, and shell elements were used for the serpentine-shaped PI/metal/PI layers. The maximum strain in the metal layer is well below tensile limit, 1% under 15% stretch of the optofluidic probe.

Fabrication of base station

A flexible sheet of copper-clad PI (Cu/PI/Cu, 18 μm/75 μm/18 μm; DuPont, Pyralux) served as the substrate. The transmission coil and interdigitated electrodes were defined on both sides with an ultraviolet laser cutting tool (ProtoLaser U4, LPKF, Germany). Holes (diameter, 50 μm) were drilled through the substrate using the same tool. Pulsed direct-current electroplating of copper filled the sidewall of these holes to define electrical connections between the top and bottom layers. The interdigitated electrodes were coated with gold (200 nm) by electroless plating to prevent oxidation of the copper in the presence of KOH solution. The critical electronic components, including a capacitor (02016D225MAT2A, AVX Corporation), a rectifier (SMS7621-040LF, Skyworks Solutions Inc.), an indicator (APG0603SURC-TT, Kingbright Company LLC), and a microcontroller (ATTINY84A-MU, Microchip Technology), were then placed and attached using reflow soldering with a low-temperature solder (Indium Corporation). The μ-ILED probe was aligned and soldered onto the electronic base station using a low-temperature solder. A layer of epoxy (thickness, ~500 μm; Loctite Epoxy Marine) applied as an overcoat prevented delamination of the electronic components. The final step of the fabrication involved application of a uniform encapsulation bilayer of parylene (14 μm; Specialty Coating Systems) and PDMS (~200 μm, dip coating).

Preparation of the metal/Al_2O_3 membrane

Fabrication began with a PI film (thickness, 12.5 μm) with a layer of Cu/Au (thickness, 250 nm/150 nm) formed by electron beam evaporation (e-beam evaporator, AJA International). The metal-coated PI film was then laminated on a clean glass slide (length, 75 mm; width, 50 mm; thickness, 1 mm) (Corning Microscope Slides, Corning, NY, USA), with a coating of PDMS formed by spin-coating (1000 rpm for 60 s) followed by curing at 70°C for 1 hour. Photolithography (AZ 4620, AZ Electronic Materials) and reactive ion etching defined a metal membrane (radius, ~1.2 mm; thickness, 400 nm) supported by a PI film (fig. S11). Last, atomic layer deposition formed a layer of aluminum oxide (Al_2O_3; thickness, 25 nm) on the metal membrane.

Preparation of flexible membrane

The fabrication began with dissolution of SBS (Sigma-Aldrich, MO, USA) in toluene with sonication. The SBS solution (4 g/40 ml) was then cast on a silicon wafer pretreated with mold release spray (Ease Release 200, Mann Release Technologies Inc., PA, USA) for 5 min and then annealed at 60°C (~3 hours) and then at 95°C (overnight). A bilayer of Ti/SiO_2 (5 nm/20 nm) deposited by sputtering (AJA International) rendered the surface of the SBS film hydrophilic.

Fabrication of the micropump chamber and pharmacological agent reservoir

Fabrication of the micropump chamber and drug reservoir involved milling a block of COP (thickness, 1 mm). Deposition of a bilayer of Ti/SiO_2 (5 nm/50 nm) by sputtering (AJA International) onto the

inner surface of the reservoir rendered it hydrophilic to facilitate filling with aqueous solutions.

Assembly of the device

Schematic illustrations of the assembly of the device are shown in fig. S12. Cylindrical micropump chambers patterned in the COP were aligned to the interdigitated electrodes and bonded with a commercially available sealant (3M marine adhesive sealant fast cure 5200) to prevent evaporation or leakage of electrolyte. The flexible membrane of SBS (~150 μm) was attached on the bottom of the reservoirs with a pressure-sensitive adhesive (Adhesives Research Inc., EL-8932EE). The reservoirs in the COP were aligned on the micropump chamber and bonded using the same sealant (3M marine adhesive sealant fast cure 5200). The metal/Al_2O_3 membrane (thickness, 400 nm/25 nm; radius, ~1.2 mm) was mounted on the four outlets of the reservoirs using the same double-sided pressure-sensitive adhesive to seal the device and prevent fluid evaporation. The inlets of the microfluidic probe were aligned and bonded to the outlet ports of the reservoirs using the same double-sided pressure-sensitive adhesive. The μ-ILED probe and microfluidic channels were aligned and bonded with a silicone adhesive (Kwik-Sil, World Precision Instruments). Last, a soft PDMS cuff was bonded with the optofluidic probe using the same silicone adhesive.

Animal testing

All procedures were approved by the Animal Care and Use Committee of Washington University and were in strict accordance with the U.S. National Institutes of Health (NIH) *Guide for the Care and Use of Laboratory Animals*. Adult male mice (8 to 14 weeks of age) used in experiments were housed in the Washington University School of Medicine animal facilities on a 12-hour light/dark cycle with access ad libitum to food and water.

For relevant optogenetic experiments, mice were generated with conditional expression of ChR2 in nociceptive sensory neurons by crossing heterozygous TRPV1-Cre mice [provided by M. Hoon (National Institute of Dental and Craniofacial Research)] (*42*) with homozygous Ai32 mice harboring ChR2 in the Rosa locus (stock no. 012569, the Jackson laboratory) (*43*). For the purposes of this study, we refer to these mice as "TRPV1-ChR2." These mice are further characterized in the work of Park *et al.* (*18*). Heterozygous Ai32 mice (Cre-negative mice) were used as controls. All other experiments were performed using C57BL/6J mice bred in-house or obtained from the Jackson laboratory.

Procedures for implantation

Mice were anesthetized with vaporized isoflurane, and their eyes were covered with Altalube ointment (Altaire Pharmaceuticals, Riverhead, NY, USA) to prevent corneal drying. A small skin incision was made over the greater trochanter of the femur on the left flank of the animals. The fascia connecting the biceps femoris and the gluteus maximus was blunt-dissected apart to open a plane between the muscles, in which the sciatic nerve was clearly accessible. A skin incision was made on the thoracic curve of the vertebral column and a subcutaneous pocket generated by blunt dissection. The body of the device was inserted under the skin into the subcutaneous pocket and sutured in place using an Ethicon 4-0 vicryl suture (Cornelia, GA, USA) to the underlying muscle through eyelets on each side of the device. For sham surgeries, the sciatic nerve was exposed and isolated, but no device was implanted. To test effects of higher modulus materials, a 2-mm section of a split PE-20 PE tubing [inside diameter, 0.38 mm;outer diameter, 1.09 mm; ~0.25 GPa (*32*–*34*)] was placed around the nerve for comparison to the optofluidic cuff (*35*).

Hematoxylin and eosin histological evaluations

Two or 10 weeks after cuff implantation, mice were deeply anesthetized with a ketamine, xylazine, and acepromazine cocktail and then transcardially perfused with cold 4% paraformaldehyde in phosphate-buffered saline. Sciatic nerves were dissected from mice implanted with the device or PE cuff or from sham mice and post-fixed in 4% paraformaldehyde overnight. Nerves were embedded in paraffin and longitudinal sections were cut at 6 μm. Slides were stained with a standard hematoxylin and eosin protocol (*18*, *44*). Representative 40× images taken from the center of the nerve were obtained using a Leica DM6 B microscope, and infiltrating immune cells were counted (*18*). Three mice were analyzed for each condition, and three nerve sections were evaluated from each mouse. Two images were obtained from each nerve section, and the average number of immune cells present in the six images was calculated. The investigator performing the analysis was blinded to the experimental condition.

Behavioral analyses

For behavioral studies, a priori power analyses were performed to estimate necessary sample sizes. The experimenters were blind to genotype and treatment (device implantation versus sham versus PE cuff positive controls) for all analyses. Animals from each genotype were randomly selected for treatment.

Rotarod test

Mice were assessed for gross motor function using an accelerating Rotarod (Ugo Basile). Mice were trained until they were able to remain on the Rotarod (4 rpm) for 120 s. One hour after training, five consecutive trials were performed on an accelerating Rotarod with 5 min between trials. Latency to fall was measured as the apparatus accelerated from 4 to 40 rpm over 5 min.

Gait analysis

Gait analysis was performed using the automated gait analysis hardware (CatWalk XT 10.5, Noldus) with the standard mouse calibration (camera gain, green light intensity, run duration, and run maximum variation). All animals were acclimatized to the CatWalk system twice for 15 min, 1 day before testing. Mice were tested 2 weeks after surgical implantation of the optofluidic device/PE cuff or sham surgery). Four compliant runs were required for each mouse, and parameters were averaged. Runs were deemed compliant if the run duration was between 0.5 and 5 s (through the camera field of view) and the maximum variation in run speed was less than 60% (*45*). These criteria were previously determined to be optimal for eliminating runs where mice did not continue to move through the field of view (*45*). Any runs that did not meet these criteria were characterized by the software as noncompliant and removed from further analysis. Swing time is a measure of how long the paw was off the ground. Print area measures the total area (in cm^2) that the complete print covers during a step. Mean contact intensity is an indirect measure of paw pressure on the ground during the point of maximum contact (0 to 255).

Real-time place aversion experiments

Place aversion was tested in a custom-designed plexiglass chamber with a layer of corn cob bedding (*18*, *21*). Each arm of the two-arm

V-maze was 10 cm wide, 33 cm long, and 10 cm high with a neutral area between the two arms. The signal was generated in one arm only by tethering the designated arm with a double loop antenna. The signal was attenuated to allow for complete local field coverage and precise control of μ-ILED device power within the designated arm. Each mouse was placed in the neutral area of the chamber, and activity was continuously recorded using a video camera for a period of 20 min. "Time in chamber" and heat maps were generated for data using EthoVision software (Noldus, Leesburg, VA, USA). The μ-ILED device was instantaneously and automatically switched to the "ON" state each time the mouse entered into the double-loop antenna–equipped arm. Similarly, the μ-ILED device was automatically switched to the "OFF" state each time the mouse exited the antenna-equipped arm. Software and hardware for generating the signal were from NeuroLux Inc. (Champaign, IL, USA).

Hargreaves test

Animals were acclimated on a glass plate held at 30°C (model 390 series 8, IITC Life Science Inc.). A radiant heat source was applied to the hindpaw, and latency to paw withdrawal was recorded (*46*). Three trials were conducted on each paw, with at least 5 min between testing the opposite paw and at least 10 min between testing the same paw. To avoid tissue damage, a cutoff latency of 20 s was set. Values from each paw were averaged to determine withdrawal latency.

Statistical analysis

All experiments were performed on adult male mice (8 to 14 weeks of age) and were randomly assigned to control or experimental groups and device implantation. Sample sizes were determined from preliminary experiments using the software G*Power for the appropriate type of statistical comparison. For place preference and thermal sensitivity assays, data were excluded from animals where the device was obviously damaged. All data were collected in a nonbiased manner, and the experimenter was blinded to treatment for histological analysis and to animal genotype for the place preference assay. One-way and two-way analyses of variance (ANOVAs) were performed as appropriate. P values <0.05 were considered statistically significant. All graphs are represented as means ± SEM. Further statistical details can be found in tables S3 and S4.

SUPPLEMENTARY MATERIALS

Supplementary material for this article is available at http://advances.sciencemag.org/cgi/content/full/5/7/eaaw5296/DC1

Note S1. Pressure in the pump chamber and drug reservoir.
Note S2. Models for the radius of the cuff.
Note S3. Analytical model of contact pressure between the nerve and the cuff.
Note S4. Oxygen and hydrogen permeability of the flexible SBS membrane.
Note S5. Mechanical characterizations of optofluidic probe.
Note S6. Flow rate measurement.
Fig. S1. Images of the wireless electronics and the complete system.
Fig. S2. Detailed images of the electrochemical micropump.
Fig. S3. Modulus and water permeability of the flexible SBS membrane.
Fig. S4. Computational results for pressure in the pump chamber and the drug reservoir as a function of volume of drug delivered from the system.
Fig. S5. Demonstration of drug loading and device reuse.
Fig. S6. Mechanical properties of the soft opotofluidic probe.
Fig. S7. Measurements of nerve temperature during various μ-ILED illumination protocols.
Fig. S8. Diagrams of formation of cuff from bilayer PDMS strips.
Fig. S9. Mechanical characterizations of cuff.
Fig. S10. Demonstration of the dye delivery via the optofluidic cuff 2 weeks after implantation and the positive control PE tubing cuff implantation.
Fig. S11. Schematic illustrations of the metal membrane on the PI substrate.
Fig. S12. Schematic illustrations of the assembly of device.
Fig. S13. Isochoric gas permeation system.
Table S1. Oxygen and hydrogen permeability of the flexible SBS membrane.
Table S2. Fabrication process details.
Table S3. Statistical results for Fig. 3.
Table S4. Statistical results for Fig. 4.
Movie S1. The deformation of the flexible membrane.
Movie S2. The flow of fluid from the reservoir.
Movie S3. Mouse with a blue μ-LED during exercise on a running wheel.
Reference (*47*)

REFERENCES AND NOTES

1. E. S. Boyden, F. Zhang, E. Bamberg, G. Nagel, K. Deisseroth, Millisecond-timescale, genetically targeted optical control of neural activity. *Nat. Neurosci.* **8**, 1263–1268 (2005).
2. A. Canales, X. Jia, U. P. Froriep, R. A. Koppes, C. M. Tringides, J. Selvidge, C. Lu, C. Hou, L. Wei, Y. Fink, P. Anikeeva, Multifunctional fibers for simultaneous optical, electrical and chemical interrogation of neural circuits in vivo. *Nat. Biotechnol.* **33**, 277–284 (2015).
3. C. Dagdeviren, K. B. Ramadi, P. Joe, K. Spencer, H. N. Schwerdt, H. Shimazu, S. Delcasso, K.-i. Amemori, C. Nunez-Lopez, A. M. Graybiel, M. J. Cima, R. Langer, Miniaturized neural system for chronic, local intracerebral drug delivery. *Sci. Transl. Med.* **10**, eaan2742 (2018).
4. K. Deisseroth, Optogenetics. *Nat. Methods* **8**, 26–29 (2011).
5. E. Iseri, D. Kuzum, Implantable optoelectronic probes for in vivo optogenetics. *J. Neural Eng.* **14**, 031001 (2017).
6. T.-i. Kim, J. G. McCall, Y. H. Jung, X. Huang, E. R. Siuda, Y. H. Li, J. Z. Song, Y. M. Song, H. A. Pao, R.-H. Kim, C. F. Lu, S. D. Lee, I.-S. Song, G. Shin, R. Al-Hasani, S. Kim, M. P. Tan, Y. G. Huang, F. G. Omenetto, J. A. Rogers, M. R. Bruchas, Injectable, cellular-scale optoelectronics with applications for wireless optogenetics. *Science* **340**, 211–216 (2013).
7. B. P. Timko, M. Arruebo, S. A. Shankarappa, J. B. McAlvin, O. S. Okonkwo, B. Mizrahi, C. F. Stefanescu, L. Gomez, J. Zhu, A. Zhu, J. Santamaria, R. Langer, D. S. Kohane, Near-infrared-actuated devices for remotely controlled drug delivery. *Proc. Natl. Acad. Sci. U.S.A.* **111**, 1349–1354 (2014).
8. O. Yizhar, L. E. Fenno, T. J. Davidson, M. Mogri, K. Deisseroth, Optogenetics in neural systems. *Neuron* **71**, 9–34 (2011).
9. R. H. Kramer, A. Mourot, H. Adesnik, Optogenetic pharmacology for control of native neuronal signaling proteins. *Nat. Neurosci.* **16**, 816–823 (2013).
10. J.-W. Jeong, J. G. McCall, G. Shin, Y. H. Zhang, R. Al-Hasani, M. Kim, S. Li, J. Y. Sim, K.-I. Jang, Y. Shi, D. Y. Hong, Y. H. Liu, G. P. Schmitz, L. Xia, Z. B. He, P. Gamble, W. Z. Ray, Y. G. Huang, M. R. Bruchas, J. A. Rogers, Wireless optofluidic systems for programmable in vivo pharmacology and optogenetics. *Cell* **162**, 662–674 (2015).
11. K. Deisseroth, Optogenetics: 10 years of microbial opsins in neuroscience. *Nat. Neurosci.* **18**, 1213–1225 (2015).
12. F. Zhang, V. Gradinaru, A. R. Adamantidis, R. Durand, R. D. Airan, L. de Lecea, K. Deisseroth, Optogenetic interrogation of neural circuits: Technology for probing mammalian brain structures. *Nat. Protoc.* **5**, 439–456 (2010).
13. T. D. Y. Kozai, N. B. Langhals, P. R. Patel, X. Deng, H. Zhang, K. L. Smith, J. Lahann, N. A. Kotov, D. R. Kipke, Ultrasmall implantable composite microelectrodes with bioactive surfaces for chronic neural interfaces. *Nat. Mater.* **11**, 1065–1073 (2012).
14. I. R. Minev, P. Musienko, A. Hirsch, Q. Barraud, N. Wenger, E. M. Moraud, J. Gandar, M. Capogrosso, T. Milekovic, L. Asboth, R. F. Torres, N. Vachicouras, Q. H. Liu, N. Pavlova, S. Duis, A. Larmagnac, J. Vörös, S. Micera, Z. G. Suo, G. Courtine, S. P. Lacour, Electronic dura mater for long-term multimodal neural interfaces. *Science* **347**, 159–163 (2015).
15. D. R. Sparta, A. M. Stamatakis, J. L. Phillips, N. Hovelsø, R. van Zessen, G. D. Stuber, Construction of implantable optical fibers for long-term optogenetic manipulation of neural circuits. *Nat. Protoc.* **7**, 12–23 (2012).
16. J. K. Nguyen, D. J. Park, J. L. Skousen, A. E. Hess-Dunning, D. J. Tyler, S. J. Rowan, C. Weder, J. R. Capadona, Mechanically-compliant intracortical implants reduce the neuroinflammatory response. *J. Neural Eng.* **11**, 056014 (2014).
17. K. L. Montgomery, A. J. Yeh, J. S. Ho, V. Tsao, S. M. Iyer, L. Grosenick, E. A. Ferenczi, Y. Tanabe, K. Deisseroth, S. L. Delp, A. S. Y. Poon, Wirelessly powered, fully internal optogenetics for brain, spinal and peripheral circuits in mice. *Nat. Methods* **12**, 969–974 (2015).
18. S.-I. Park, D. S. Brenner, G. Shin, C. D. Morgan, B. A. Copits, H. U. Chung, M. Y. Pullen, K. N. Noh, S. Davidson, S. J. Oh, J. Yoon, K. I. Jang, V. K. Samineni, M. Norman, J. G. Grajales-Reyes, S. K. Vogt, S. S. Sundaram, K. M. Wilson, J. S. Ha, R. X. Xu, T. S. Pan, T.-i. Kim, Y. G. Huang, M. C. Montana, J. P. Golden, M. R. Bruchas, R. W. Gereau, J. A. Rogers, Soft, stretchable, fully implantable miniaturized optoelectronic systems for wireless optogenetics. *Nat. Biotechnol.* **33**, 1280–1286 (2015).
19. G. Shin, A. M. Gomez, R. Al-Hasani, Y. R. Jeong, J. Kim, Z. Q. Xie, A. Banks, S. M. Lee, S. Y. Han, C. J. Yoo, J. L. Lee, S. H. Lee, J. Kurniawan, J. Tureb, Z. Z. Guo, J. Yoon, S. I. Park, S. Y. Bang, Y. Nam, M. C. Walicki, V. K. Samineni, A. D. Mickle, K. Lee, S. Y. Heo, J. G. McCall, T. S. Pan, L. Wang, X. Feng, T.-i. Kim, J. K. Kim, Y. H. Li, Y. G. Huang, R. W. Gereau, J. S. Ha,

M. R. Bruchas, J. A. Rogers, Flexible near-field wireless optoelectronics as subdermal implants for broad applications in optogenetics. *Neuron* **93**, 509–521.e3 (2017).
20. V. K. Samineni, J. Yoon, K. E. Crawford, Y. R. Jeong, K. C. McKenzie, G. Shin, Z. Q. Xie, S. S. Sundaram, Y. H. Li, M. Y. Yang, J. Kim, D. Wu, Y. G. Xue, X. Feng, Y. G. Huang, A. D. Mickle, A. Banks, J. S. Ha, J. P. Golden, J. A. Rogers, R. W. Gereau, Fully implantable, battery-free wireless optoelectronic devices for spinal optogenetics. *Pain* **158**, 2108–2116 (2017).
21. V. K. Samineni, A. D. Mickle, J. Yoon, J. G. Grajales-Reyes, M. Y. Pullen, K. E. Crawford, K. N. Noh, G. B. Gereau, S. K. Vogt, H. H. Lai, J. A. Rogers, R. W. Gereau IV, Optogenetic silencing of nociceptive primary afferents reduces evoked and ongoing bladder pain. *Sci. Rep.* **7**, 15865 (2017).
22. J. Kim, A. Banks, H. Y. Cheng, Z. Q. Xie, S. Xu, K.-I. Jang, J. W. Lee, Z. J. Liu, P. Gutruf, X. Huang, P. H. Wei, F. Liu, K. Li, M. Dalal, R. Ghaffari, X. Feng, Y. G. Huang, S. Gupta, U. Paik, J. A. Rogers, Epidermal electronics with advanced capabilities in near-field communication. *Small* **11**, 906–912 (2015).
23. P. Gutruf, V. Krishnamurthi, A. Vázquez-Guardado, Z. Xie, A. Banks, C.-J. Su, Y. Xu, C. R. Haney, E. A. Waters, I. Kandela, S. R. Krishnan, T. Ray, J. P. Leshock, Y. Huang, D. Chanda, J. A. Rogers, Fully implantable optoelectronic systems for battery-free, multimodal operation in neuroscience research. *Nat. Electron.* **1**, 652–660 (2018).
24. C. G. Cameron, M. S. Freund, Electrolytic actuators: Alternative, high-performance, material-based devices. *Proc. Natl. Acad. Sci. U.S.A.* **99**, 7827–7831 (2002).
25. A. Cobo, R. Sheybani, E. Meng, MEMS: Enabled drug delivery systems. *Adv. Healthc. Mater.* **4**, 969–982 (2015).
26. H. Gensler, R. Sheybani, P.-Y. Li, R. Lo Mann, E. Meng, An implantable MEMS micropump system for drug delivery in small animals. *Biomed. Microdevices* **14**, 483–496 (2012).
27. E. Meng, T. Hoang, MEMS-enabled implantable drug infusion pumps for laboratory animal research, preclinical, and clinical applications. *Adv. Drug Deliv. Rev.* **64**, 1628–1638 (2012).
28. P. S. Nunes, P. D. Ohlsson, O. Ordeig, J. P. Kutter, Cyclic olefin polymers: Emerging materials for lab-on-a-chip applications. *Microfluid. Nanofluid.* **9**, 145–161 (2010).
29. I. Piskarev, V. Ushkanov, N. Aristova, P. Likhachev, T. Myslivets, Establishment of the redox potential of water saturated with hydrogen. *Biophysics* **55**, 13–17 (2010).
30. J. A. Beel, D. E. Groswald, M. W. Luttges, Alterations in the mechanical properties of peripheral nerve following crush injury. *J. Biomech.* **17**, 185–193 (1984).
31. P. S. Yarmolenko, E. J. Moon, C. Landon, A. Manzoor, D. W. Hochman, B. L. Viglianti, M. W. Dewhirst, Thresholds for thermal damage to normal tissues: An update. *Int. J. Hyperthermia* **27**, 320–343 (2011).
32. S. P. Lacour, G. Courtine, J. Guck, Materials and technologies for soft implantable neuroprostheses. *Nat. Rev. Mater.* **1**, 16063 (2016).
33. J. Rivnay, H. Wang, L. Fenno, K. Deisseroth, G. G. Malliaras, Next-generation probes, particles, and proteins for neural interfacing. *Sci. Adv.* **3**, e1601649 (2017).
34. R. F. Landel, L. E. Nielsen, *Mechanical Properties of Polymers and Composites* (CRC Press, 1993).
35. I. Yalcin, S. Megat, F. Barthas, E. Waltisperger, M. Kremer, E. Salvat, M. Barrot, The sciatic nerve cuffing model of neuropathic pain in mice. *J. Vis. Exp.* **2014**, 51608 (2014).
36. K. N. Noh, S. I. Park, R. Qazi, Z. N. Zou, A. D. Mickle, J. G. Grajales-Reyes, K.-I. Jang, R. W. Gereau IV, J. L. Xiao, J. A. Rogers, J.-W. Jeong, Miniaturized, battery-free optofluidic systems with potential for wireless pharmacology and optogenetics. *Small* **14**, 1702479 (2018).
37. K. Kandler, T. Nguyen, J. Noh, R. S. Givens, An optical fiber-based uncaging system. *Cold Spring Harb. Protoc.* **2013**, 118–121 (2013).
38. S. Park, Y. Y. Guo, X. T. Jia, H. K. Choe, B. Grena, J. Kang, J. Park, C. Lu, A. Canales, R. Chen, Y. S. Yim, G. B. Choi, Y. Fink, P. Anikeeva, One-step optogenetics with multifunctional flexible polymer fibers. *Nat. Neurosci.* **20**, 612–619 (2017).
39. S. Balasubramaniam, S. A. Wirdatmadja, M. T. Barros, Y. Koucheryavy, M. Stachowiak, J. M. Jornet, Wireless communications for optogenetics-based brain stimulation: Present technology and future challenges. *IEEE Commun. Mag.* **56**, 218–224 (2018).
40. P. Gutruf, J. A. Rogers, Implantable, wireless device platforms for neuroscience research. *Curr. Opin. Neurobiol.* **50**, 42–49 (2018).
41. L. Birder, W. de Groat, I. Mills, J. Morrison, K. Thor, M. Drake, Neural control of the lower urinary tract: Peripheral and spinal mechanisms. *Neurourol. Urodyn.* **29**, 128–139 (2010).
42. S. K. Mishra, S. M. Tisel, P. Orestes, S. K. Bhangoo, M. A. Hoon, TRPV1-lineage neurons are required for thermal sensation. *EMBO J.* **30**, 582–593 (2011).
43. L. Madisen, T. Y. Mao, H. Koch, J.-m. Zhuo, A. Berenyi, S. Fujisawa, Y.-W. A. Hsu, A. J. Garcia III, X. Gu, S. Zanella, J. Kidney, H. Gu, Y. M. Mao, B. M. Hooks, E. S. Boyden, G. Buzsaki, J. M. Ramirez, A. R. Jones, K. Svoboda, X. Han, E. E. Turner, H. K. Zeng, A toolbox of Cre-dependent optogenetic transgenic mice for light-induced activation and silencing. *Nat. Neurosci.* **15**, 793–802 (2012).
44. A. H. Fischer, K. A. Jacobson, J. Rose, R. Zeller, Hematoxylin and eosin staining of tissue and cell sections. *Cold Spring Harb. Protoc.* **2008**, pdb.prot4986 (2008).
45. A. J. Shepherd, D. P. Mohapatra, Pharmacological validation of voluntary gait and mechanical sensitivity assays associated with inflammatory and neuropathic pain in mice. *Neuropharmacology* **130**, 18–29 (2018).
46. K. Hargreaves, R. Dubner, F. Brown, C. Flores, J. Joris, A new and sensitive method for measuring thermal nociception in cutaneous hyperalgesia. *Pain* **32**, 77–88 (1988).
47. T. T. Moore, S. Damle, P. J. Williams, W. J. Koros, Characterization of low permeability gas separation membranes and barrier materials; design and operation considerations. *J. Membr. Sci.* **245**, 227–231 (2004).

Acknowledgments: We would like to thank J. Sinn-Hanlon of the Design Group at VetMed, University of Illinois at Urbana-Champaign for the illustrations. This work used the Northwestern University Micro/Nano Fabrication Facility (NUFAB), which is partially supported by Soft and Hybrid Nanotechnology Experimental (SHyNE) Resource (NSF ECCS-1542205). This work made use of the MatCI Facility, which receives support from the MRSEC Program (NSF DMR-1720139) of the Materials Research Center at Northwestern University. **Funding:** This work was funded by an NIH Director's Transformative Research Award TR01 NS081707 (to R.W.G. and J.A.R.), NIH SPARC Award via the NIBIB of the NIH award U18EB021793 (to R.W.G. and J.A.R.), R01 NS42595 (to R.W.G.), NIMH of the NIH under Award Number R41MH116525, NRSA F32 DK115122 (to A.D.M.), the McDonnell Center for Cellular and Molecular Neurobiology Postdoctoral Fellowship (to A.D.M.), T32 DA007261 (to L.A.M.), the Medical Scientist Training Program (MSTP) Grant T32 GM07200 and NINDS NRSA F31 NS103472 (to J.G.G.-R.), and the University of Missouri-Columbia start-up fund (to Y.Z.). **Author contributions:** Y.Z., A.D.M., P.G., and L.A.M. contributed equally to the work; Y.Z., A.D.M., P.G., L.A.M., J.A.R., and R.W.G. conceived of and designed experiments/material devices; Y.Z., H.G., Y.W., P.G., Y.X., D.P., C.-J.S., and S.K. designed and provided optofluidic cuff devices; Y.Z., P.G., H.G., Y.W., X.W., F.Z., and J.T.R. conducted all benchtop tests; Y.X. and Y.H. contributed to mechanical modeling; A.D.M. and L.A.M. performed all surgical implantations; A.D.M., L.A.M., and J.P.G. collected and analyzed histological data; A.D.M., L.A.M., J.P.G., S.K.V., and J.G.G.-R. performed and analyzed data from all behavioral experiments; Y.Z., A.D.M., L.A.M., J.A.R., and R.W.G. wrote the manuscript. **Competing interests:** J.A.R. and R.W.G. are cofounders of NeuroLux, a company that manufactures wireless optoelectronic devices. The NeuroLux commercial hardware system was used in conjunction with custom software in the present study to control activity of the optofluidic system. The authors declare no other competing interests. **Data and materials availability:** All data needed to evaluate the conclusions in the paper are present in the paper and/or the Supplementary Materials. Additional data related to this paper may be requested from the authors.

Submitted 4 January 2019
Accepted 29 May 2019
Published 5 July 2019
10.1126/sciadv.aaw5296

Citation: Y. Zhang, A. D. Mickle, P. Gutruf, L. A. McIlvried, H. Guo, Y. Wu, J. P. Golden, Y. Xue, J. G. Grajales-Reyes, X. Wang, S. Krishnan, Y. Xie, D. Peng, C.-J. Su, F. Zhang, J. T. Reeder, S. K. Vogt, Y. Huang, J. A. Rogers, R. W. Gereau IV, Battery-free, fully implantable optofluidic cuff system for wireless optogenetic and pharmacological neuromodulation of peripheral nerves. *Sci. Adv.* **5**, eaaw5296 (2019).

Science Advances

Battery-free, fully implantable optofluidic cuff system for wireless optogenetic and pharmacological neuromodulation of peripheral nerves

Yi Zhang, Aaron D. Mickle, Philipp Gutruf, Lisa A. McIlvried, Hexia Guo, Yixin Wu, Judith P. Golden, Yeguang Xue, Jose G. Grajales-Reyes, Xueju Wang, Siddharth Krishnan, Yiwen Xie, Dongsheng Peng, Chun-Ju Su, Fengyi Zhang, Jonathan T. Reeder, Sherri K. Vogt, Yonggang Huang, John A. Rogers and Robert W. Gereau IV

Sci Adv **5** (7), eaaw5296.
DOI: 10.1126/sciadv.aaw5296